remote sensing

MDPI

Article

Hydraulics of Time-Variable Water Surface Slope in Rivers Observed by Satellite Altimetry

Peter Bauer-Gottwein [1,2,*], Linda Christoffersen [3], Aske Musaeus [1,4], Monica Coppo Frías [1] and Karina Nielsen [3]

[1] Department of Environmental and Resource Engineering, Technical University of Denmark, 2800 Kongens Lyngby, Denmark
[2] Department of Geosciences and Natural Resource Management, University of Copenhagen, 1958 Frederiksberg, Denmark
[3] National Space Center, Technical University of Denmark, 2800 Kongens Lyngby, Denmark
[4] DHI, 2970 Hørsholm, Denmark
* Correspondence: pbg@ign.ku.dk

Abstract: The ICESat-2 and SWOT satellite earth observation missions have provided highly accurate water surface slope (WSS) observations in global rivers for the first time. While water surface slope is expected to remain constant in time for approximately uniform flow conditions, we observe time varying water surface slope in many river reaches around the globe in the ICESat-2 record. Here, we investigate the causes of time variability of WSSs using simplified river hydraulic models based on the theory of steady, gradually varied flow. We identify bed slope or cross section shape changes, river confluences, flood waves, and backwater effects from lakes, reservoirs, or the ocean as the main non-uniform hydraulic situations in natural rivers that cause time changes of WSSs. We illustrate these phenomena at selected river sites around the world, using ICESat-2 data and river discharge estimates. The analysis shows that WSS observations from space can provide new insights into river hydraulics and can enable the estimation of river discharge from combined observations of water surface elevation and WSSs at sites with complex hydraulic characteristics.

Keywords: river hydraulics; satellite altimetry; ICESat-2; water surface slope; river discharge

check for updates

Citation: Bauer-Gottwein, P.; Christoffersen, L.; Musaeus, A.; Frías, M.C.; Nielsen, K. Hydraulics of Time-Variable Water Surface Slope in Rivers Observed by Satellite Altimetry. *Remote Sens.* **2024**, *16*, 4010. https://doi.org/10.3390/rs16214010

Academic Editor: Konstantinos X. Soulis

Received: 22 August 2024
Revised: 24 October 2024
Accepted: 27 October 2024
Published: 29 October 2024

Copyright: © 2024 by the authors. Licensee MDPI, Basel, Switzerland. This article is an open access article distributed under the terms and conditions of the Creative Commons Attribution (CC BY) license (https://creativecommons.org/licenses/by/4.0/).

1. Introduction

Satellite radar and laser altimetry have developed into mature techniques to monitor the Earth's inland waters. A review paper by an international team of altimetry experts [1] provides an overview of available missions, databases, and data processing approaches. Many global rivers have been investigated using satellite altimetry datasets [2–5], and satellite altimetry has been incorporated into operational hydrologic-hydraulic modelling and forecasting workflows [6–9]. ICESat-2 [10] and SWOT [11] are unique among satellite altimetry missions because they do not only provide river water surface elevation (WSE) at the cross-over points between a river and the satellite ground track (so-called virtual stations) but also provide observations of local water surface slopes (WSSs, i.e., the slope of the water surface along the river [12,13]). The mapping of river WSS at the regional to global scale reveals that the WSS is constant in time in many river reaches but varies significantly over time in other river reaches. The main factor causing the time variability of WSE and WSS in rivers is the river discharge, which varies according to the weather and rainfall-runoff response in the contributing catchment and can change by a factor of 100 or more in highly seasonal rivers. In uniform river reaches, increased river discharge leads to increased WSE, while the WSS remains unchanged. This unique relationship between the WSE and discharge forms the basis for many algorithms estimating river discharge from satellite altimetry observations (e.g., [14–18]). However, in non-uniform hydraulic conditions, the WSS changes significantly with river discharge and observed changes

in the WSS provide new insights into the hydraulic phenomena occurring in such river reaches. Here, we classify typical non-uniform flow situations in natural rivers, in which time-variable river WSS occurs. We develop simplified hydraulic models for each of these typical non-uniform flow situations using the classic theory of steady gradually varied flow [19]. We select one river site for each of the typical non-uniform flow situations and illustrate the inter-relations between river discharge, WSE, and WSS using river discharge records from in-situ monitoring networks or reanalysis in combination with ICESat-2 WSE and WSS datasets.

2. Methods and Data

We first classify typical non-uniform flow situations that occur in natural rivers. Subsequently, we explain how these situations can be modelled using the classic theory of steady gradually varied one-dimensional flow outlined in the textbook by Ven Te Chow [19]. We then describe how ICESat-2 data were processed into river water surface elevation and water surface slope and how river discharge was estimated. All data processing and modelling workflows were implemented in Python version 3.12.

2.1. Typical Non-Uniform Flow Situations in Natural Rivers

Under the assumptions of steady, uniform flow, the water surface slope is equal to bed slope and does not change with discharge. Thus, the WSS remains constant in time as illustrated in Figure 1A. Steady uniform flow occurs in long river reaches with constant discharge, uniform cross section shape, uniform hydraulic roughness, and uniform bed slope. While steady uniform flow is a reasonable approximation in many situations, we identified four common non-uniform flow situations in natural rivers that cause the WSS to change with discharge and thus in time: (1) changes of bed slope, cross section shape, and/or hydraulic roughness along the river—i.e., conveyance changes (Figure 1B). If conveyance changes abruptly, we predict a characteristic backwater profile upstream of the change. The shape of the dimensionless backwater profile is invariant under discharge changes (see modelling section), while the dimensional water surface elevation and water surface slope profiles change with discharge. This non-uniform flow situation commonly occurs upstream of waterfalls or rapids (Figure 1B1)—i.e., upstream of river cross sections with critical flow. (2) River confluences. As described in [20] and illustrated in Figure 1C, low flow in one tributary can coincide with high flow in the other tributary and vice versa, leading to significant WSS variability in the backwater affected zones upstream of the confluence in both tributaries. (3) Flood waves traveling through a river reach. Traveling waves cause high WSS during the passage of the wavefront and low WSS in front and in the wake of the flood wave (Figure 1D). (4) Backwater effects from lakes, reservoirs, or the ocean. Water level changes in the receiving water bodies propagate upstream into the tributary river, causing WSS changes in the backwater-affected zone (Figure 1E). At sites of type A, we expect time-constant WSS, while at sites of types B-E, we expect the WSS to change with discharge and thus in time. We will now discuss how each of these typical non-uniform flow situations can be modelled using the theory of steady gradually varied one-dimensional flow.

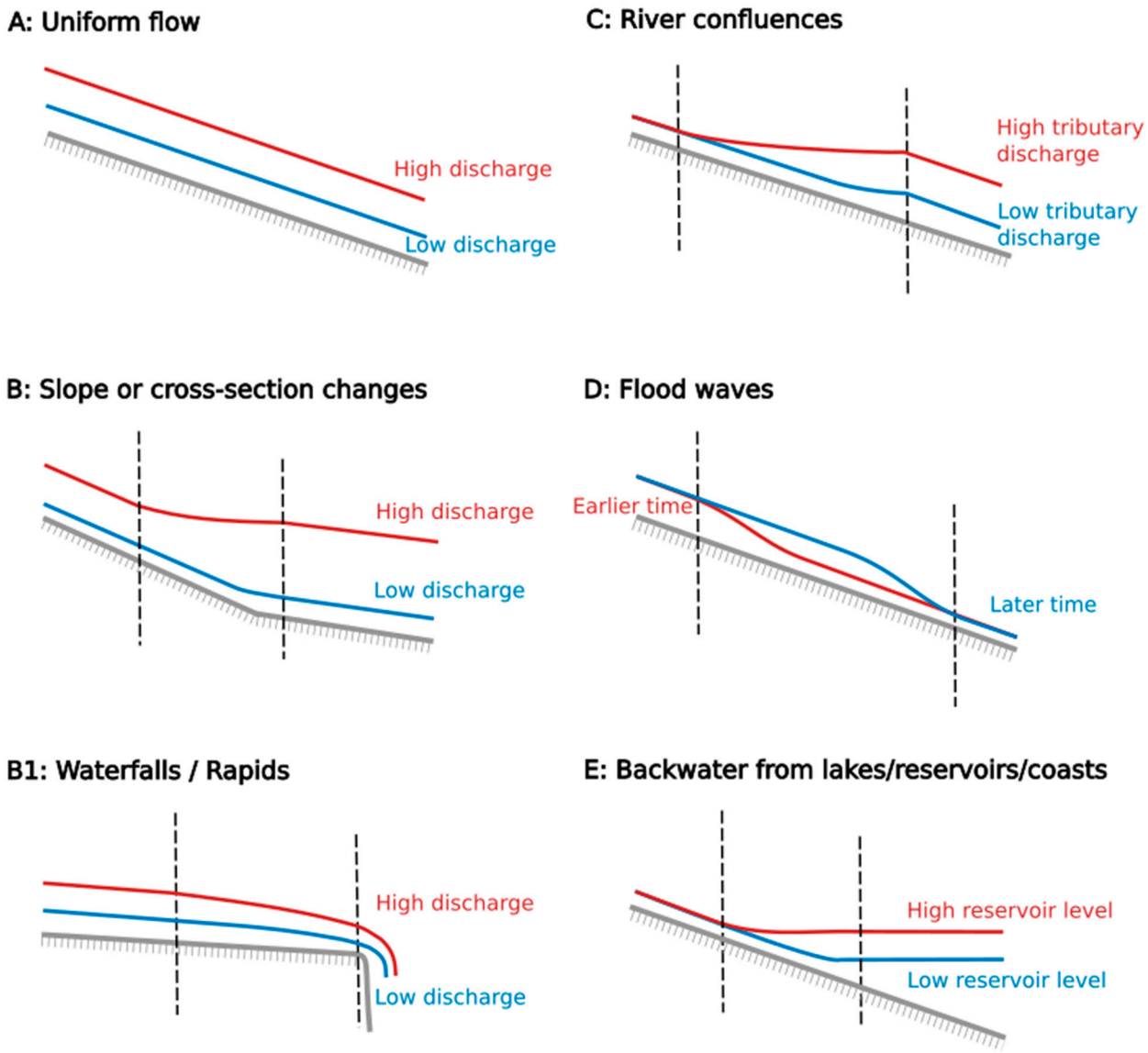


Figure 1. Hydraulic phenomena causing time-variable water surface slope in rivers. Vertical dashed lines delineate the zone of significant WSS change. (**A**) River reach with uniform flow. (**B**) Abrupt conveyance change. (**B1**) Waterfalls or rapids. (**C**) Reaches upstream of river confluences. (**D**) Flood waves traveling through the river reach. (**E**) Backwater effects upstream of lakes, reservoirs, or the ocean.

2.2. Modeling River Water Surface Elevation and Slope Using Steady Gradually Varied Flow Model

We modelled the water surface elevation and water surface slope in the typical non-uniform flow situations shown in Figure 1 using the theory of steady gradually varied one-dimensional flow as explained in detail in the classic hydraulics textbook by Chow [19] (chapter 9). This modelling approach is highly simplified and does not capture the complexities of natural river flow in detail. We thus expect qualitative agreement between the derived models and the observations but do not expect the models to fit the observations. Despite these limitations and because of its highly simplified nature, this modeling approach provides generic insights into the inter-relations of water surface elevation, water surface slope, and river discharge in the typical non-uniform flow situations described above.

In this modelling framework, the water surface elevation upstream of an anomalous region can be described using the steady-state version of the one-dimensional De Saint-Venant equations for flow in open channels. The equation reads as

$$\frac{dy}{dx} = \frac{S_0 - S_f}{1 - Fr^2} \tag{1}$$

where y is the water depth in the river, x is the chainage, S_0 is the bed slope, S_f is the friction slope, and Fr is Froude's number—i.e., the ratio of the flow velocity and the velocity of gravity waves in shallow water. Using Chézy's parameterization of the friction slope for a wide river with width b and friction coefficient C, i.e., $S_f = Q^2 b^{-2} C^{-2} y^{-3}$, and introducing the normalized depth $u = y/y_n$, we obtain (see Chow [19] (p. 222)),

$$y_n \frac{du}{dx} = S_0 \frac{u^3 - 1}{u^3 - y_c^3/y_n^3} \tag{2}$$

where y_n is the normal depth, $y_n = \left(Q^2 b^{-2} C^{-2} S_0^{-1}\right)^{1/3}$, and y_c is the critical depth, $y_c = \left(Q^2 b^{-2} g^{-1}\right)^{1/3}$. Normal depth, or steady uniform flow depth, is the depth in a long river reach with uniform discharge, cross section shape, bed slope, and hydraulic roughness. The Chézy coefficient varies with river characteristics. A widely accepted default value for large rivers is 90 $m^{1/2}/s$. We use this default value throughout this paper but acknowledge that the coefficient varies from site to site in reality and should be determined using an inverse modeling approach for detailed site-scale hydraulic modeling. For a given boundary condition u_b at the anomalous region, the depth profile upstream of the anomalous region can be calculated analytically as ([19] p. 254)

$$x = \frac{y_n}{S_0}\left[\left(u - \left[1 - \frac{C^2 S_0}{g}\right]F(u)\right) - \left(u_b - \left[1 - \frac{C^2 S_0}{g}\right]F(u_b)\right)\right] \tag{3}$$

with $F(u) = \frac{1}{6}\ln\left(\frac{u^2+u+1}{(u-1)^2}\right) + \frac{1}{\sqrt{3}}\arctan\left(\frac{2u+1}{\sqrt{3}}\right)$, enabling the calculation of the chainage point corresponding to any normalized depth u in the river. Note that once depth is known, water surface elevation can be calculated as bottom elevation plus depth, and water surface slope can be calculated as $WSS = S_0 - dy/dx$, where dy/dx directly results from Equation (1).

The different situations illustrated in Figure 1 can now be understood in terms of different boundary conditions u_b in the application of Equation (3). In all cases, we assume that flow is at normal depth downstream of the anomalous region—i.e., for the simulation of the water depth upstream of the anomalous region, depth at the boundary is equal to normal depth in the downstream reach. Case A implies that friction slope and bed slope remain equal across the entire domain, and thus water surface slope does not vary with discharge or chainage and is always equal to the bed slope, independent of the discharge in the river. Using Chézy's equation for the friction slope, steady uniform flow results in a rating relationship between depth and discharge given by the normal flow equation.

In case B, the boundary condition u_b becomes equal to the ratio between the normal depths in the downstream and upstream portions of the river: $u_b = y_{n,d}/y_{n,u}$. In the case of the slope break, $u_b = \left(Q^2 b^{-2} C^{-2} S_{0,\mathrm{d}}^{-1}\right)^{1/3} / \left(Q^2 b^{-2} C^{-2} S_{0,\mathrm{u}}^{-1}\right)^{1/3} = (S_{0,u}/S_{0,d})^{1/3}$, where $S_{0,u}$ is the upstream bed slope and $S_{0,d}$ the downstream bed slope. In the case of a cross section change (changing river width), we get $u_b = \left(Q^2 b_d^{-2} C^{-2} S_0^{-1}\right)^{1/3} / \left(Q^2 b_u^{-2} C^{-2} S_0^{-1}\right)^{1/3} = (b_u/b_d)^{2/3}$. Importantly, the boundary condition u_b in case B is independent of discharge, which implies that the shape of the water level profile remains the same but is scaled with the normal depth in the upstream reach, as evident from equation 3. In the special case B1, i.e., upstream of waterfalls and rapids, the flow goes through a critical section and the boundary

condition becomes $u_b = y_c/y_n = \left(Q^2 b^{-2} g^{-1}\right)^{1/3} / \left(Q^2 b^{-2} C^{-2} S_0^{-1}\right)^{1/3} = \left(C^2 S_0/g\right)^{1/3}$, which is again independent of discharge. The critical section is located at some distance (a few tens of meters) upstream of the fall [21], but for reach-scale analysis, it can be assumed that the critical section is at the location of the waterfall.

In case C, the boundary condition u_b becomes equal to the ratio between the normal depth downstream of the confluence and the normal depth upstream of the confluence: $u_{b,i} = y_{n,d}/y_{n,i}$, where i can take values of one or two and indicates the two upstream tributaries. This boundary is no longer independent of discharge but depends on the relative magnitude of both tributary discharges: $u_{b,i} = y_{n,d}/y_{n,i} = \left((Q_1 + Q_2)^2 {b_d}^{-2} {C_d}^{-2} S_{0,d}^{-1} / ({Q_i}^2 {b_i}^{-2} {C_i}^{-2} S_{0,i}^{-1}) \right)^{1/3}$. The same confluence model is also presented in [20].

Case D is a dynamic phenomenon, and the water surface elevation and water surface slope changes quickly in time as the flood wave sweeps through the river reach. An analytical traveling wave model (called uniformly progressive flow in [19]) exists for the case of a flood wave traveling through a long uniform river reach [19] (pp. 528–535). While the assumption of a traveling wave may be a significant simplification in most cases, the analytical model provides a useful estimate of the maximum water surface slope occurring at the wave front. The traveling wave model reads as

$$\frac{dy}{dx} = S_0 \frac{(y - y_1)(y - y_2)(y - y_3)}{y_3 - q_0^2/g} \tag{4}$$

Here, y_1 is the depth far upstream of the wave front, y_2 is the depth far downstream of the wavefront, $y_3 = q_0^2 C^{-2} S_0^{-1} y_1^{-1} y_2^{-1}$, and $q_0 = y_1 y_2 (v_1 - v_2)(y_1 - y_2)^{-1}$. Flow velocities upstream and downstream of the wave front can be calculated with Chézy's formula as $v_i = C S_0^{1/2} y_i^{1/2}$. An implicit analytical solution for the depth exists:

$$x = 1/S_0 \cdot \left[\left(y + ln\left[(y_1 - y)^{\alpha} \cdot (y - y_2)^{\beta} \cdot (y - y_3)^{\gamma} \right] \right) - \left(y_0 + ln\left[(y_1 - y_0)^{\alpha} \cdot (y_0 - y_2)^{\beta} \cdot (y_0 - y_3)^{\gamma} \right] \right) \right] \tag{5}$$

Here, $y_0 = \frac{y_1 + y_2}{2}$ is the depth at chainage $x = 0$ (where chainage is defined in a coordinate system that moves with the speed of the wave front), $\alpha = \left(y_1^3 - y_c^3\right)(y_1 - y_2)^{-1}(y_1 - y_3)^{-1}$, $\beta = \left(y_c^3 - y_2^3\right)(y_1 - y_2)^{-1}(y_2 - y_3)^{-1}$, $\gamma = \left(y_3^3 - y_c^3\right)(y_1 - y_3)^{-1}(y_2 - y_3)^{-1}$, and $y_c = \left(q_0^2/g\right)^{1/3}$. Moreover, we can find the maximum WSS and the depth at maximum WSS by solving

$$\frac{d}{dy}\left(\frac{dy}{dx}\right) = \frac{d}{dy}\left(S_0 \frac{(y - y_1)(y - y_2)(y - y_3)}{y_3 - q_0^2/g} \right) = 0 \tag{6}$$

which leads to a 4-th order equation in y with one real root in the range between y_1 and y_2. The maximum WSS can then be calculated by plugging the selected root into equation 4 and adding the bed slope. This result is useful because it enables us to estimate the maximum water surface slope occurring during the passage of a wave front as dependent on the water level change across the front and river characteristics.

In case E, the boundary condition u_b is entirely dependent on the water level in the lake, reservoir, or ocean into which the river flows and does not only depend on river discharge. Depending on the water level in the receiving water body, the backwater profile will propagate upstream to a larger or lesser extent, which will lead to significant water surface slope changes in the backwater-affected zone of the river.

2.3. Processing of ATL03 Water Surface Elevation Data

In this section, we explain how the water surface elevation and water surface slope were derived from the ICESat-2 data products. We derived water surface elevation and water surface slope estimates from the ICESat-2 ATL03 product, version 6 [22,23]. Coppo Frías

et al. [24] describe the processing of ICESat-2 data for river modelling in detail. ICESat-2 ATL03 version 6 data were downloaded, re-projected to the local UTM coordinate system, re-referenced to the EGM08 global geoid model [25], and assigned to the river-following one-dimensional coordinate (chainage). Individual photon return coordinates were also projected to the cross section coordinates perpendicular to the river. River overflights (Figure 2A) were cleaned, and only high quality and high confidence photon events were retained. Subsequently, overflight photons were classified in a histogram with 30 bins per meter, and the bin with the highest photon count was identified (Figure 2B). The water surface elevation was then estimated as the average of all photon events falling between the highest photon count plus/minus 0.3 m. The water surface slope was calculated as the ratio of differences in water surface elevation at the cross-over points of the six individual ICESat-2 ground tracks and corresponding differences in river chainage at the cross-over points.

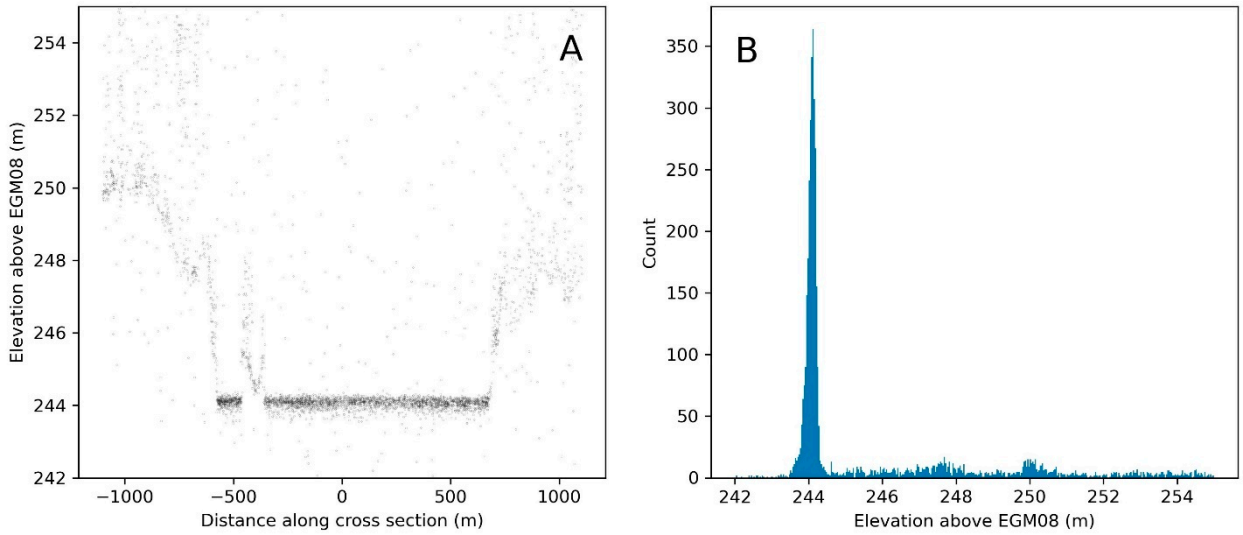


Figure 2. Processing of ATL03 river crossings. Example river crossing of the Peace River near Vermillion Falls on 3 June 2019 (ATL03 file name: ATL03_20190306160236_10420202_006_02_gt1l). (**A**): ATL03 elevation points along the cross section. (**B**): Histogram of ATL03 heights along cross section.

2.4. River Discharge Estimates

River discharge varies strongly in time for most rivers and is the dominant force changing the WSE and WSS in rivers. We need river discharge estimates to analyze the interrelations of river discharge, WSE, and WSS. Ideally, this analysis should be conducted using in-situ observations of river discharge only because the accuracy of in-situ observations is higher than that of estimates derived from models and reanalysis systems. However, in-situ, station-based river discharge estimates are scarce, and data are not publicly shared in many countries. In this study, in-situ river discharge observations for the days of ICESat-2 overpasses were extracted from the Global Runoff Data Center (GRDC) global runoff database [26] for the sites for which observations were available in the GRDC archive. For sites without available GRDC records, we extracted discharge reanalysis data from the River Discharge and Related Forecasted Data archive produced by the Global Flood Awareness System (GLOFAS) and archived on the Copernicus Data Store [27,28]. These reanalysis estimates are based on the GLOFAS global runoff model and are informed with historical in-situ observations. The uncertainty of GLOFAS reanalysis discharge is expected to be significantly higher than the uncertainty of GRDC in-situ river discharge, but we cannot quantify uncertainty for individual river sites and observation times. To extract GLOFAS time series, daily gridded discharge estimates were downloaded from the archive and pixel values for the river sites of interest were extracted and compiled into time series.

3. Results

Sites corresponding to the typical non-uniform flow situations shown in Figure 1 were identified on global rivers based on the literature, inspection of satellite imagery, and inspection of ICESat-2 ATL03 datasets from the sites. Sites of type A can typically be found at or close to established in-situ gauging stations because such stations require a simple and stable rating curve. We chose the Pfelling gauging station on the Danube River in Germany as an example of sites of type A.

Sites of type B are not very common because a natural river tends to smooth out abrupt changes of slope and cross section shape by erosion and sedimentation processes. Bed slope changes from high slope to low slope are typically not abrupt but gradual, smoothing out backwater effects generated by the slope change, as illustrated for the Torne River on the border between Sweden and Finland in Figure 3.

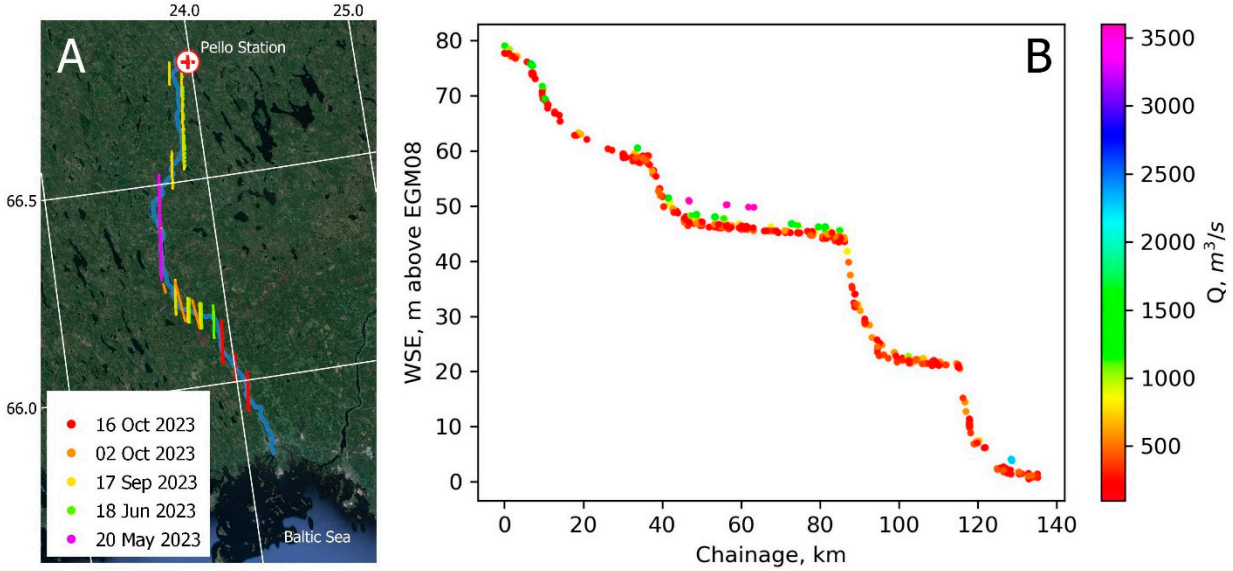


Figure 3. ATL03 water surface elevation profile for the Torne River. (**A**): Base map of the area with selected ICESat-2 tracks. Background is Google satellite imagery. Coordinate grid as decimal latitude and longitude (EPSG 4326). (**B**): ICESat-2 WSE data versus river km from Pello. Pink datapoints are from 20 May 2023. Pello in-situ discharge data [29] show a 100-year flood event on this day.

However, rapids and waterfalls (case B1) are common in rivers around the world and can be easily identified on high-resolution imagery as sections with whitewater. Here we use the example of the Vermilion Falls on the Peace River in Canada to illustrate this non-uniform flow situation.

Many major river confluences (case C) exist on the global river network. We chose the Ganges-Ghaghara confluence close to the city of Chapra in India to illustrate the hydraulic phenomena around river confluences. Liu et al., 2023 [20] show similar results for a number of major river confluences in the Mississippi-Missouri river system.

Flood waves (case D) are short-term phenomena and, because of the sparse temporal sampling pattern, are hard to observe in the ICESat-2 record. A spectacular flood wave was generated by the June 2023 dam break of the Kakhovka Dam on the Dnipro River in Ukraine [30]. Coincidentally, ICESat-2 provided one high-quality overpass over the area affected by the flood wave on 6 June 2023 in the immediate aftermath of the dam break. We use this case to illustrate the impact of flood waves on the water surface slope in rivers.

Backwater upstream of lakes and reservoirs is a common phenomenon around the world, as there are thousands of major reservoirs on world rivers that show significant seasonal water level variations. We choose the Toktogul reservoir on the Naryn River in Kyrgyzstan here to illustrate this phenomenon. Coastal backwater affects all rivers as

they approach the oceans. However, this phenomenon is more complex because tidal variations at the coastal water level are fast, leading to dynamic changes of water surface elevation profiles in coastal rivers including flow reversals and anti-slopes, which cannot be modelled using the concept of steady gradually varied flow and are thus beyond the scope of this paper.

3.1. Case A: Uniform Flow

A typical uniform flow site is the Pfelling gauging station (Lon: 12.7472, Lat: 48.8797) on the Danube River in Germany (Figure 4). In-situ discharge data are available from the GRDC online database [26] and has been used in this analysis. Figure 4 illustrates the available ICESat-2 crossings and the location of the in-situ station. Panel B provides ICESat-2 water surface elevation estimates as dependent on chainage and river discharge. We observe a close match between the observed water surface elevations and the water surface elevations predicted by the uniform flow equation. Panels C and D provide observed water surface elevations and water surface slopes for the in-situ station location as well as simulated WSE–discharge and WSS–discharge relationships. The WSE observations along the river were extrapolated to the station location assuming a uniform WSS. It is evident that the data are in good qualitative agreement with the uniform flow assumption—i.e., increasing WSE with discharge, following a power law, and a uniform WSS with discharge. In summary, in case A, we expect increasing WSE with increasing discharge and a constant WSS with increasing discharge. ICESat-2 data from the Pfelling site are in qualitative agreement with this conceptual understanding.

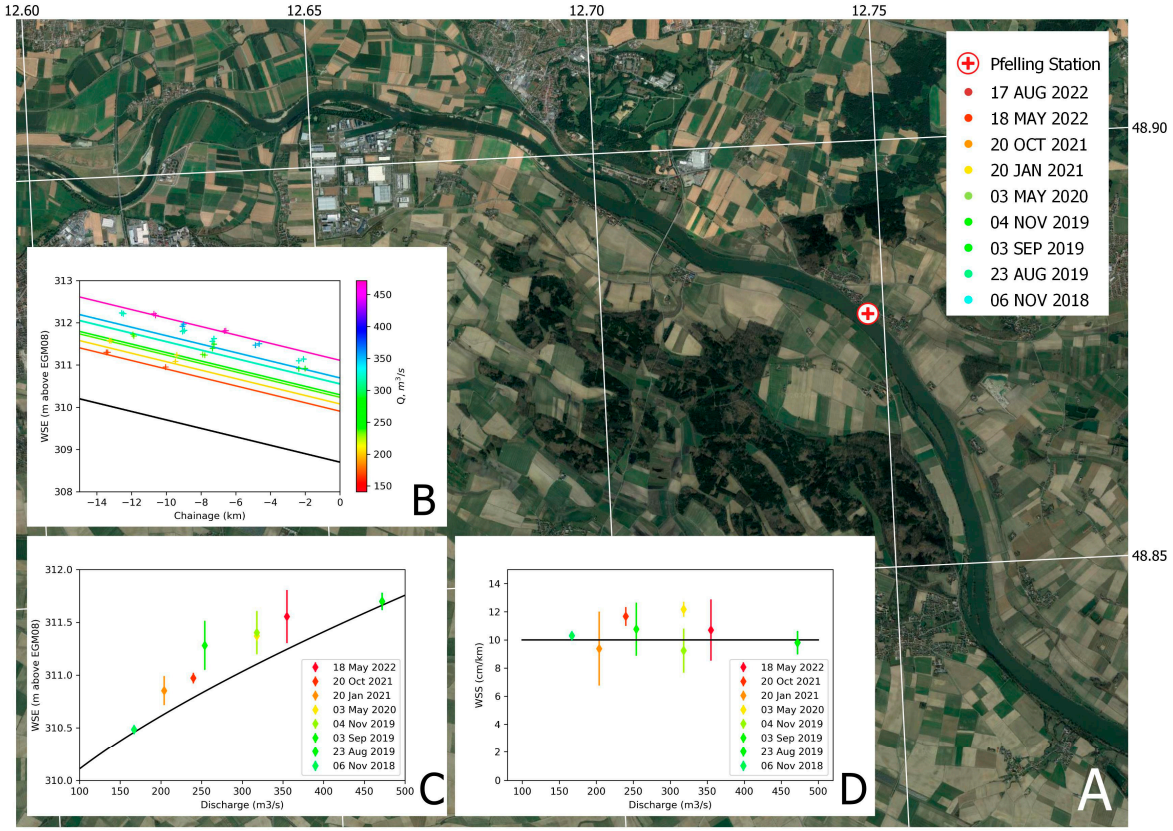


Figure 4. Uniform flow at the Pfelling site on the Danube River. (**A**): Base map of the area and available ICESat-2 overpasses. Background is Google satellite imagery. Coordinate grid as decimal latitude and longitude (EPSG 4326). (**B**): Simulated (solid lines) and ICESat-2 (crosses) WSE as dependent on GRDC discharge. Black solid line is imputed river bottom elevation. (**C**): Simulated (solid line) and observed WSE at Pfelling station. Vertical lines indicate 90% confidence intervals. (**D**): Simulated (solid line) and observed WSS at Pfelling station. Vertical lines indicate 90% confidence intervals.

3.2. Case B: Slope or Cross Section Change

We illustrate case B1 for the Vermillion falls (Lon: −114.8707, Lat: 58.3713) on the Peace River in Canada (Figure 5). This river section is fairly uniform but bisected by a waterfall of several meters' altitude, as shown in panels A and B of Figure 5. We excluded ICESat-2 data for the winter months (November to March) as the river is icebound in this period, which complicates water level–discharge relationships. We do not have access to in-situ river discharge at this site and thus used the GLOFAS reanalysis dataset [27,28] to estimate river discharge. Significant river discharge uncertainty is thus to be expected. Panel B shows good qualitative agreement of the ICESat-2 data with a hydraulic model simulating a critical flow section just upstream of the falls. Some noise exists in the discharge–WSE relationships, which we partly attribute to the limited accuracy of the GLOFAS river discharge data. As illustrated in Panel C, the hydraulic model with a critical section at the downstream boundary results in unique 1:1 relationships between the river discharge and WSE and river discharge/WSS for any chainage point upstream of the falls within the zone affected by the backwater from the falls. For this reason, observations of WSE and/or WSS can be directly translated to river discharge in this case, making it possible to estimate river discharge from space. In summary, in case B1, we expect increasing WSE and increasing WSS with increasing discharge. The ICESat-2 dataset from Vermillion Falls is in qualitative agreement with this conceptual understanding. Sites of type B1 are common in global rivers and offer good conditions for estimating river discharge from satellite earth observation using remotely sensed WSE, WSS, or a combination of both.

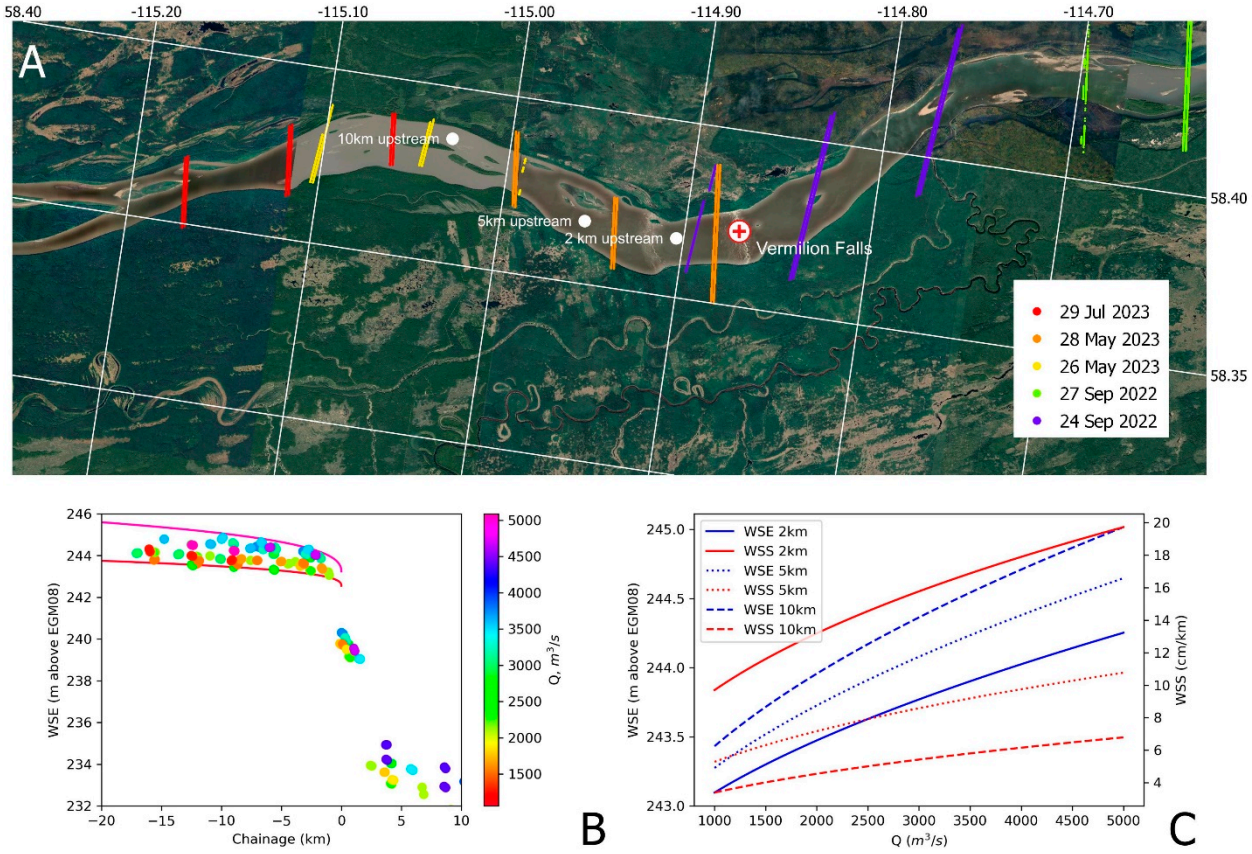


Figure 5. Vermillion Falls on the Peace River. (**A**): Base map of the area with selected ICESat-2 tracks. Background is Google satellite imagery. Coordinate grid as decimal latitude and longitude (EPSG 4326). (**B**): Simulated (solid lines) and ICESat-2 (dots) WSE as dependent on GLOFAS discharge. (**C**): Simulated WSE and WSS at three points upstream of the falls.

3.3. Case C: River Confluence

We illustrate river confluence effects at the confluence of the Ganges and Ghaghara rivers (Lon: 84.7130, Lat: 25.7371) in India in Figure 6. The discharge estimates at this site are from the GLOFAS archive [28], and we thus expect significant uncertainty in terms of the estimated discharge. The hydraulic confluence model used here is described in the methods section and in a recent paper [20]. Clearly, the ICESat-2 datasets are in qualitative agreement with the predictions provided by the confluence model, while exact quantitative matches cannot be expected given the limitations of the GLOFAS discharge estimates and the simplifying assumptions underlying the hydraulic model. In summary, upstream of river confluences, the WSE and WSS are determined by the discharges in both tributaries. Discharge in one of the tributaries only is insufficient to predict the WSE and WSS in the river. Thus, care needs to be taken when interpreting the WSE and WSS from satellite earth observation upstream of major river confluences.

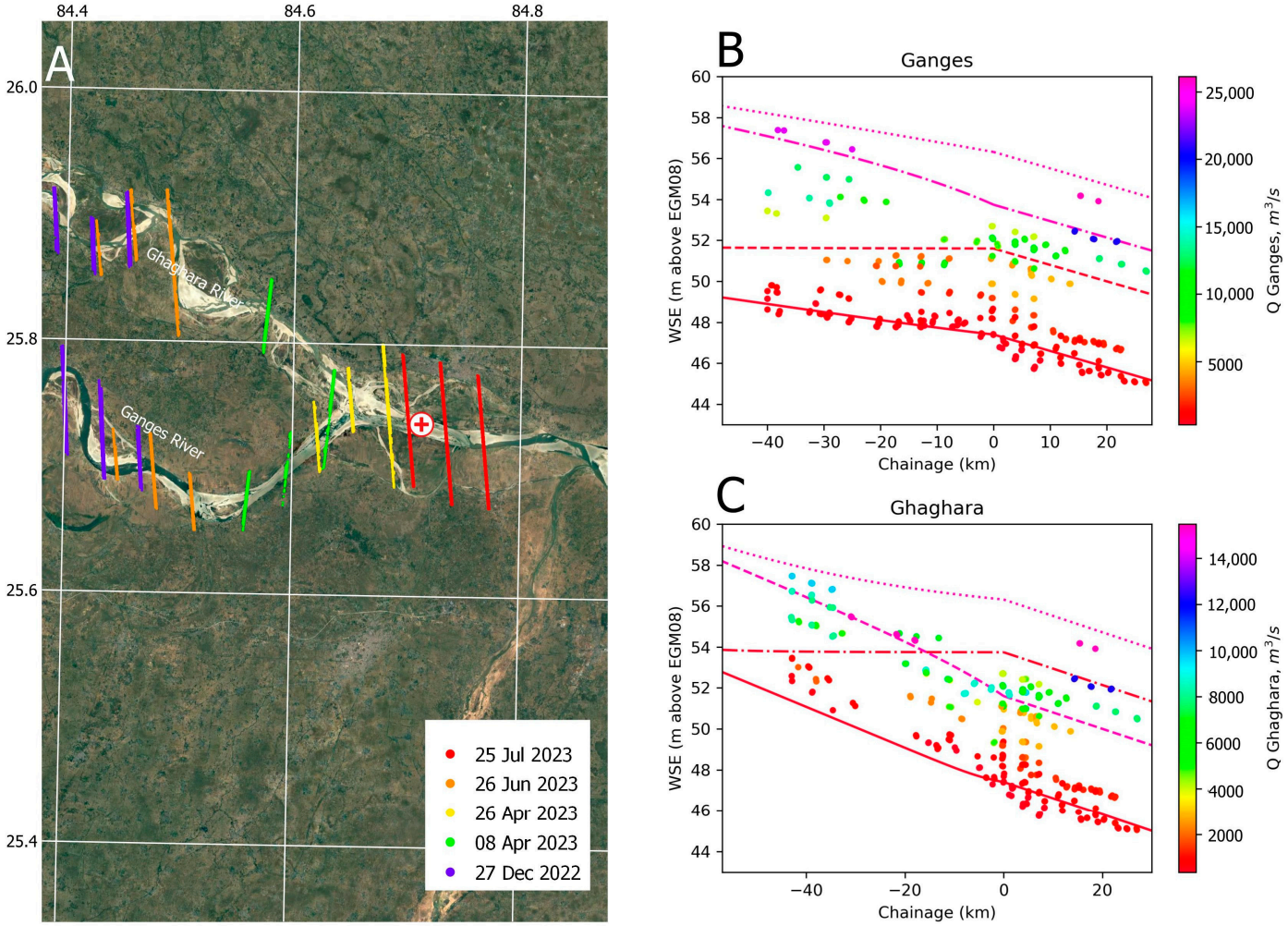


Figure 6. Confluence between the Ganges and the Ghaghara Rivers. (**A**): Base map of the area with selected ICESat-2 tracks. Background is Google satellite imagery. Coordinate grid as decimal latitude and longitude (EPSG 4326). (**B**): Simulated (lines) and ICESat-2 (dots) WSE in the Ganges as dependent on Ganges River discharge (GLOFAS). (**C**): Simulated (lines) and ICESat-2 (dots) WSE in the Ghaghara as dependent on Ghaghara River discharge (GLOFAS). In (**B**,**C**), solid lines indicate simulation results for minimum flow in both Ganges and Ghaghara, dotted lines indicate maximum flow in both Ganges and Ghaghara, dashed lines indicate minimum flow in Ganges and maximum flow in Ghaghara, and dashed-dotted lines indicate maximum flow in Ghaghara and minimum flow in Ganges.

3.4. Case D: Flood Wave

On 6 June 2023, the Kakhovka dam on the Dnipro River in Ukraine (Lon: 33.3657, Lat: 46.7760) collapsed, creating a massive flood wave on the river reach from Kakhovka to the Black Sea. Water levels just downstream of the dam rose up to 16 m [30]. Several high-quality ICESat-2 tracks over the river reach are available for the period of interest, including one crossing on 6 June immediately after the dam break, as shown in Figure 7A. From the ICESat-2 data, it is evident that water levels in the river rose by several meters because of the dam break (Figure 7B) and that the water surface slope increased significantly during the flooding event at locations close to the wavefront (Figure 7C). We used the traveling wave model presented in the methods section to predict water surface slope changes around the wavefront. Assuming a bed slope of 2 cm/km, a Chézy coefficient of 90 $m^{1/2}/s$, and an effective depth of 0.5 m prior to the flood event, the model predicts a WSS change from 2 cm/km to ca. 12 cm/km during the passage of the wave front, which travels down the river at 1.7 m/s. The available ICESat-2 data show the WSS at around 20 cm/km on 6 June 2023, which is higher than the prediction of the traveling wave model and indicates that the shape of the wavefront is not in steady state at the time and place of the ICESat-2 overpass. The WSS in July–August 2023 is close to zero, indicating quasi-stagnant water (Figure 7C). In summary, the Kakhovka case shows that the range of WSS occurring during the passage of a flood wave can be predicted using the simple traveling wave model presented here. This result can be used for large-scale hydraulic analysis using SWOT and ICESat-2 data, for instance, to predict the maximum expected WSS during the passage of flood waves in global river reaches.

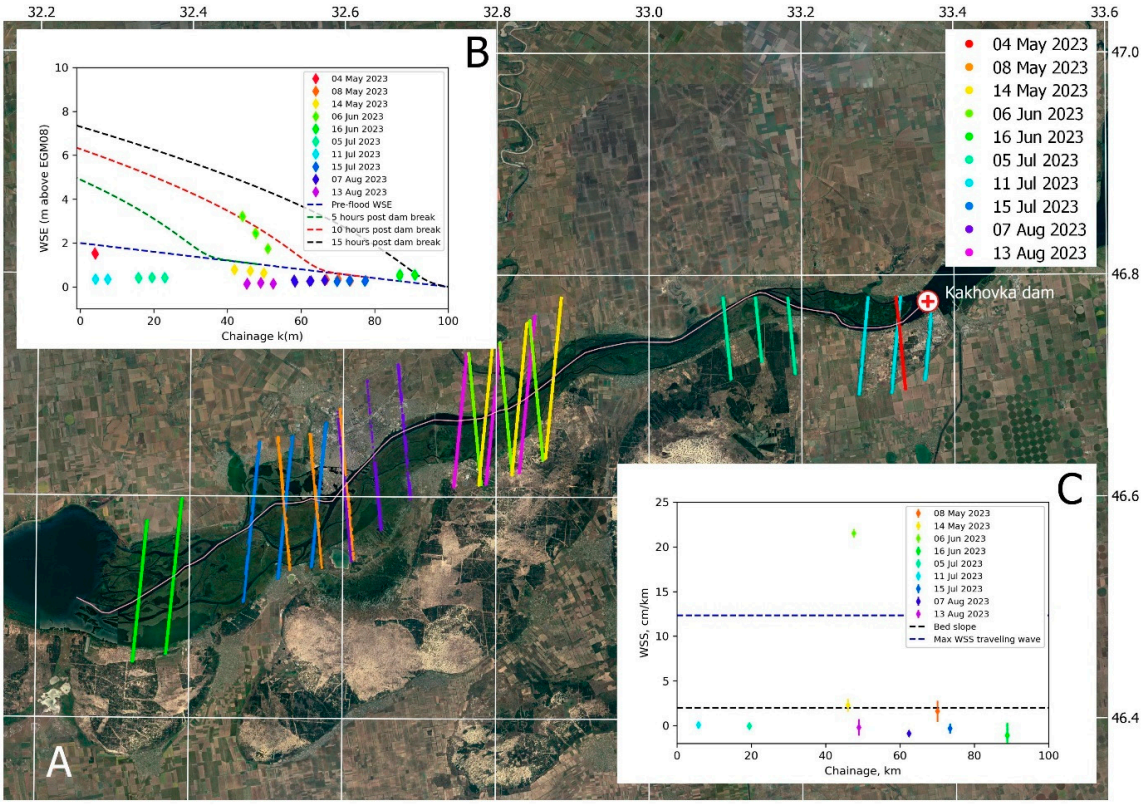


Figure 7. Dnipro River downstream of Kakhovka Dam. (**A**): Base map of the area and available ICESat-2 overpasses. Background is Google satellite imagery. Coordinate grid as decimal latitude and longitude (EPSG 4326). (**B**): ICESat-2 WSE data. Dashed lines indicate simulated propagation of the traveling wave through the river. (**C**): ICESat-2 WSS estimates with 90% confidence intervals. Dashed lines indicate bed slope (black) and maximum slope predicted by the traveling wave model (blue).

3.5. Case E: Backwater from Lakes/Reservoirs/the Coast

We illustrate the backwater effects from reservoirs for the Toktogul Reservoir on the Naryn River (Lon: 73.2568, Lat: 41.7755) in Kyrgyzstan (Figure 8). Seasonal water level changes in this reservoir are several 10s of meters, leading to significant WSS changes in the backwater-affected zones upstream of the reservoir. The ICESat-2 WSE observations show the reservoir storage dynamics (Figure 8B), and Figure 8C clearly shows the zone of high WSS variability at the interface between river and reservoir. In the downstream portion, i.e., for chainages larger than −5 km, the WSS is always close to zero as this part is always covered by the lake. In the upstream portion, i.e., for chainages between −30 km and −20 km, the WSS is always close to the bed slope of the Naryn River. In river reaches like this one, the water surface elevation and water surface slope are primarily controlled by reservoir storage dynamics, and estimating river discharge from water level is thus problematic and error prone. In summary, WSE and WSS dynamics upstream of reservoirs, lakes, and the sea are shown to depend both on river discharge and water level in the receiving water body. It is important to note that the backwater effects from receiving water bodies can extend far upstream up to hundreds of kilometers in lowland rivers with low bed slopes.

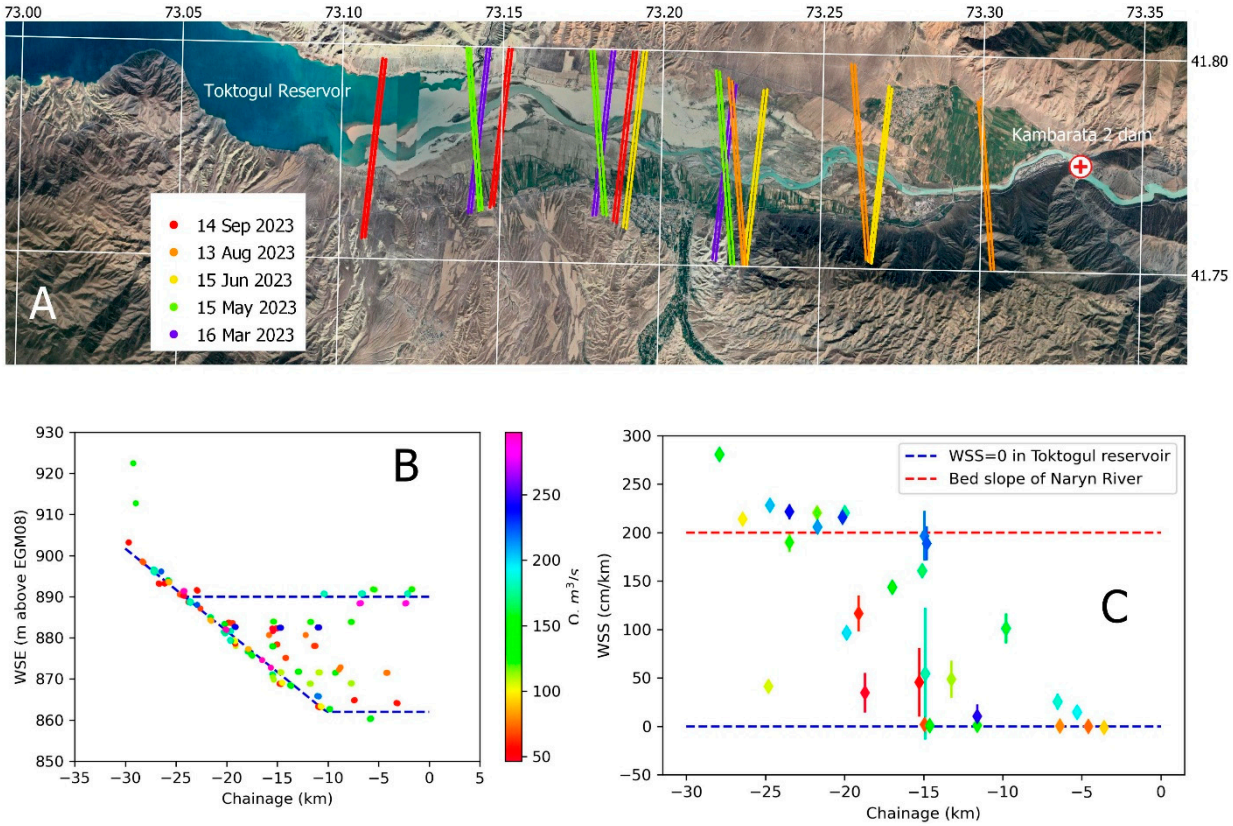


Figure 8. Toktogul Reservoir on the Naryn River. (**A**): Base map of the area with selected ICESat-2 tracks. Background is Google satellite imagery. Coordinate grid as decimal latitude and longitude (EPSG 4326). (**B**): ICESat-2 WSE data. Dashed lines indicate simulated WSE for high and low reservoir levels. (**C**): ICESat-2 WSS estimates with 90% confidence intervals. Dashed lines indicate bed slope of Naryn River and zero WSS in the reservoir.

4. Discussion

We classified non-uniform flow situations in natural rivers, analyzed the inter-relations between river discharge, water surface elevation, and water surface slope for the different non-uniform flow situations using steady gradually varied one-dimensional flow theory, and illustrated the different non-uniform flow situations using ICESat-2 laser altimetry data.

We did not perform high-fidelity hydraulic modeling in this study for two reasons: First, we do not have access the required datasets such as bathymetric surveys, accurate high-frequency discharge time series, etc., for the sites of interest. Second, we are interested in the generic inter-relations between river discharge, WSE, and WSS and not in site-specific phenomena. Due to the highly simplified nature of the hydraulic models used in this study, we do not expect to fit the observations quantitatively—i.e., we do not expect that simulated quantities are within the confidence intervals of observations. To obtain reliable high-fidelity hydraulic models of the river sites discussed in this paper, follow-up modeling studies using common numerical hydraulic modeling software packages are recommended.

4.1. Hydraulic Insights from WSS Observations

The water surface slope estimates provided by the latest generation of satellite radar and laser altimetry missions (ICESat-2, SWOT) provide detailed insights into site-scale hydraulic phenomena occurring in the investigated rivers. Specifically, analyzing the variability of WSS observations in time, we can establish the validity of the uniform flow assumptions at any river site. If uniform flow is a reasonable assumption for a site, the WSS is expected to be independent of river discharge and thus constant in time. We have outlined the most common situations in which the uniform flow assumptions are not fulfilled in natural rivers: abrupt conveyance changes, confluences, flood waves, and backwater effects from lakes/reservoirs. The simplified hydraulic models presented here enable us to produce informed estimates of the expected maximum WSS during the passage of a flood wave, the WSS changes upstream of rapids and waterfalls, and the expected WSS dynamics upstream of river confluences.

4.2. River Discharge from WSE and WSS

A key objective of current inland water altimetry research is to estimate river discharge from space. Based on our analysis, we can conclude that river discharge can be estimated from the WSE alone in cases A and B, while this was not possible in cases C, D, and E. In case C, coincident observations of WSE and WSS can lead to a well constrained discharge estimate as shown in [20], while in cases D and E, additional information is required for river discharge estimation. It is important to note that, while the WSS is independent of discharge in case A, the WSS will change with discharge in case B. We highlight again that river discharge estimates used in this study were adopted from the cited data sources without quality assurance or verification. While we are unable to quantify river discharge uncertainty for the different sites discussed in this study, we expect significant uncertainty on the order of 20–30% for the GLOFAS river discharge estimates.

4.3. Limitations of Current Observation Technology and Future Potential

Currently, the WSS can be observed with a standard error of ca 2 cm/km in rivers using ICESat-2 data [12,13]. Similar accuracy is expected from a SWOT. While this accuracy is sufficient for the study of many inland rivers, bed slopes in coastal rivers are often around or below 1 cm/km and WSS changes are of similar order of magnitude. Thus, the hydraulic analysis of coastal rivers, estuaries, and river deltas is currently still challenging, except for very large rivers with large sets of high-quality ICESat-2/SWOT observations covering long chainage intervals.

5. Conclusions

Under approximately uniform flow conditions, river WSS is constant and independent of discharge, and a unique relationship exists between the WSE and discharge, which enables the direct estimation of river discharge from satellite altimetry. However, the assumptions of uniform flow are not fulfilled along many river reaches globally including, for instance, upstream of bed slope or cross section changes (case B in this paper), upstream of waterfalls and rapids (case B1), upstream of river confluences (case C), during the transition of flood waves (case D), and upstream of lakes/reservoirs/the coast (case E). In

all these cases, the WSS varies with discharge. In case B/B1, although the WSS changes with discharge, a unique relationship between the WSE and discharge exists, just like under uniform flow conditions. In case C, there is no unique relationship between the WSE and discharge, but coincident observations of the WSE and WSS (such as available from ICESat and SWOT) can constrain discharge estimates. In cases D and E, it is not possible to estimate discharge from the WSE and WSS because both the WSS and WSE depend on additional variables other than local discharge at the point of observation.

Author Contributions: Conceptualization, P.B.-G.; Methodology, P.B.-G., L.C., A.M., M.C.F. and K.N.; Software, P.B.-G.; Validation, P.B.-G.; Formal analysis, P.B.-G., A.M., M.C.F. and K.N.; Data curation, L.C., A.M., M.C.F. and K.N.; Writing—original draft, P.B.-G.; Writing—review & editing, P.B.-G., L.C., A.M., M.C.F. and K.N. All authors have read and agreed to the published version of the manuscript.

Funding: This work was partly funded by Horizon Europe, contract number 101081783.

Data Availability Statement: This work is based exclusively on public domain data. ICESat-2 ATL03 data can be downloaded from https://nsidc.org/data/atl03/versions/6 (accessed on 15 August 2024). GLOFAS river discharge estimates can be downloaded from https://ewds.climate.copernicus.eu/datasets/cems-glofas-historical?tab=overview (accessed on 15 August 2024). GRDC river discharge data can be downloaded from https://portal.grdc.bafg.de/applications/public.html?publicuser=PublicUser#dataDownload/Stations (accessed on 15 August 2024).

Conflicts of Interest: The authors declare no conflicts of interest.

References

1. Abdalla, S.; Abdeh Kolahchi, A.; Ablain, M.; Adusumilli, S.; Aich Bhowmick, S.; Alou-Font, E.; Amarouche, L.; Andersen, O.B.; Antich, H.; Aouf, L.; et al. Altimetry for the Future: Building on 25 Years of Progress. *Adv. Space Res.* **2021**, *68*, 319–363. [CrossRef]
2. Paris, A.; Dias de Paiva, R.; Santos da Silva, J.; Medeiros Moreira, D.; Calmant, S.; Garambois, P.-A.; Collischonn, W.; Bonnet, M.-P.; Seyler, F. Stage-Discharge Rating Curves Based on Satellite Altimetry and Modeled Discharge in the Amazon Basin. *Water Resour. Res.* **2016**, *52*, 3787–3814. [CrossRef]
3. Papa, F.; Bala, S.K.; Pandey, R.K.; Durand, F.; Gopalakrishna, V.V.; Rahman, A.; Rossow, W.B. Ganga-Brahmaputra River Discharge from Jason-2 Radar Altimetry: An Update to the Long-Term Satellite-Derived Estimates of Continental Freshwater Forcing Flux into the Bay of Bengal. *J. Geophys. Res. Oceans* **2012**, *117*, C11. [CrossRef]
4. Michailovsky, C.I.; McEnnis, S.; Berry, P.A.M.; Smith, R.; Bauer-Gottwein, P. River Monitoring from Satellite Radar Altimetry in the Zambezi River Basin. *Hydrol. Earth Syst. Sci.* **2012**, *16*, 2181–2192. [CrossRef]
5. Jiang, L.; Nielsen, K.; Dinardo, S.; Andersen, O.B.; Bauer-Gottwein, P. Evaluation of Sentinel-3 SRAL SAR Altimetry over Chinese Rivers. *Remote. Sens. Environ.* **2020**, *237*, 111546. [CrossRef]
6. Schneider, R.; Ridler, M.-E.; Godiksen, P.N.; Madsen, H.; Bauer-Gottwein, P. A Data Assimilation System Combining CryoSat-2 Data and Hydrodynamic River Models. *J. Hydrol.* **2018**, *557*, 197–210. [CrossRef]
7. Hossain, F.; Siddique-E-Akbor, A.H.; Mazumder, L.C.; Shahnewaz, S.M.; Biancamaria, S.; Lee, H.; Shum, C.K. Proof of Concept of an Altimeter-Based River Forecasting System for Transboundary Flow inside Bangladesh. *IEEE J. Sel. Top. Appl. Earth Obs. Remote. Sens.* **2014**, *7*, 587–601. [CrossRef]
8. Chang, C.-H.; Lee, H.; Hossain, F.; Basnayake, S.; Jayasinghe, S.; Chishtie, F.; Saah, D.; Yu, H.; Sothea, K.; Du Bui, D. A Model-Aided Satellite-Altimetry-Based Flood Forecasting System for the Mekong River. *Environ. Model. Softw.* **2019**, *112*, 112–127. [CrossRef]
9. Paiva, R.C.D.; Collischonn, W.; Bonnet, M.-P.; De Gonçalves, L.G.G.; Calmant, S.; Getirana, A.; Santos Da Silva, J. Assimilating in Situ and Radar Altimetry Data into a Large-Scale Hydrologic-Hydrodynamic Model for Streamflow Forecast in the Amazon. *Hydrol. Earth Syst. Sci.* **2013**, *17*, 2929–2946. [CrossRef]
10. Markus, T.; Neumann, T.; Martino, A.; Abdalati, W.; Brunt, K.; Csatho, B.; Farrell, S.; Fricker, H.; Gardner, A.; Harding, D.; et al. The Ice, Cloud, and Land Elevation Satellite-2 (ICESat-2): Science Requirements, Concept, and Implementation. *Remote Sens. Environ.* **2017**, *190*, 260–273. [CrossRef]
11. Biancamaria, S.; Lettenmaier, D.P.; Pavelsky, T.M. The SWOT Mission and Its Capabilities for Land Hydrology. *Surv. Geophys.* **2016**, *37*, 307–337. [CrossRef]
12. Scherer, D.; Schwatke, C.; Dettmering, D.; Seitz, F. ICESat-2 Based River Surface Slope and Its Impact on Water Level Time Series From Satellite Altimetry. *Water Resour. Res.* **2022**, *58*, e2022WR032842. [CrossRef]
13. Christoffersen, L.; Bauer-Gottwein, P.; Sørensen, L.S.; Nielsen, K. ICE2WSS; An R Package for Estimating River Water Surface Slopes from ICESat-2. *Environ. Model. Softw.* **2023**, *168*, 105789. [CrossRef]
14. Tourian, M.J.; Elmi, O.; Shafaghi, Y.; Behnia, S.; Saemian, P.; Schlesinger, R.; Sneeuw, N. HydroSat: Geometric Quantities of the Global Water Cycle from Geodetic Satellites. *Earth Syst. Sci. Data* **2022**, *14*, 2463–2486. [CrossRef]

15. Leon, J.G.; Calmant, S.; Seyler, F.; Bonnet, M.-P.; Cauhopé, M.; Frappart, F.; Filizola, N.; Fraizy, P. Rating Curves and Estimation of Average Water Depth at the Upper Negro River Based on Satellite Altimeter Data and Modeled Discharges. *J. Hydrol.* **2006**, *328*, 481–496. [CrossRef]
16. Kouraev, A.V.; Zakharova, E.A.; Samain, O.; Mognard, N.M.; Cazenave, A. Ob' River Discharge from TOPEX/Poseidon Satellite Altimetry (1992-2002). *Remote. Sens. Environ.* **2004**, *93*, 238–245. [CrossRef]
17. Alsdorf, D.E.; Rodríguez, E.; Lettenmaier, D.P. Measuring Surface Water from Space. *Rev. Geophys.* **2007**, *45*, 2. [CrossRef]
18. Bjerklie, D.M.; Moller, D.; Smith, L.C.; Dingman, S.L. Estimating Discharge in Rivers Using Remotely Sensed Hydraulic Information. *J. Hydrol.* **2005**, *309*, 191–209. [CrossRef]
19. Chow, V.T. Open-Channel Hydraulics. McGraw-Hill: New York, NY, USA, 1959.
20. Liu, J.; Bauer-Gottwein, P.; Frias, M.C.; Musaeus, A.F.; Christoffersen, L.; Jiang, L. Stage-Slope-Discharge Relationships Upstream of River Confluences Revealed by Satellite Altimetry. *Geophys. Res. Lett.* **2023**, *50*, e2023GL106394. [CrossRef]
21. Christodoulou, G.C.; Noutsopoulos, G.C.; Andreou, S.A. Factors Affecting Brink Depth in Rectangular Overfalls. In *Proceedings of the Channels and Channel Control Structures*; Smith, K.V.H., Ed.; Springer: Berlin/Heidelberg, Germany, 1984; pp. 3–17.
22. Neumann, T.A.; Brenner, A.; Hancock, D.; Robbins, J.; Gibbons, A.; Lee, J.; Harbeck, K.; Saba, J.; Luthcke, S.B.; Rebold, T. *ATLAS/ICESat-2 L2A Global Geolocated Photon Data, Version 6*; NASA National Snow and Ice Data Center Distributed Active Archive Center: Boulder, CO, USA, 2023.
23. Neumann, T.A.; Martino, A.J.; Markus, T.; Bae, S.; Bock, M.R.; Brenner, A.C.; Brunt, K.M.; Cavanaugh, J.; Fernandes, S.T.; Hancock, D.W.; et al. The Ice, Cloud, and Land Elevation Satellite—2 Mission: A Global Geolocated Photon Product Derived from the Aadvanced Ttopographic Llaser Aaltimeter Ssystem. *Remote. Sens. Environ.* **2019**, *233*, 111325. [CrossRef]
24. Coppo Frias, M.; Liu, S.; Mo, X.; Nielsen, K.; Ranndal, H.; Jiang, L.; Ma, J.; Bauer-Gottwein, P. River Hydraulic Modeling with ICESat-2 Land and Water Surface Elevation. *Hydrol. Earth Syst. Sci.* **2023**, *27*, 1011–1032. [CrossRef]
25. Pavlis, N.K.; Holmes, S.A.; Kenyon, S.C.; Factor, J.K. The Development and Evaluation of the Earth Gravitational Model 2008 (EGM2008). *J. Geophys. Res. Solid Earth* **2012**, *117*, B4. [CrossRef]
26. The Global Runoff Data Centre—Data Download The Global Runoff Data Centre. Available online: https://portal.grdc.bafg.de/applications/public.html?publicuser=PublicUser#dataDownload/Stations (accessed on 8 April 2024).
27. Harrigan, S.; Zsoter, E.; Alfieri, L.; Prudhomme, C.; Salamon, P.; Wetterhall, F.; Barnard, C.; Cloke, H.; Pappenberger, F. GloFAS-ERA5 Operational Global River Discharge Reanalysis 1979-Present. *Earth Syst. Sci. Data* **2020**, *12*, 2043–2060. [CrossRef]
28. Copernicus Climate Change Service (C3S). River Discharge and Related Forecasted Data from the Global Flood Awareness System. 2020. Available online: https://ewds.climate.copernicus.eu/datasets/cems-glofas-historical?tab=overview (accessed on 15 August 2024).
29. VESI Waterinfo.Fi. Available online: https://www.vesi.fi/en/karttapalvelu/ (accessed on 12 April 2024).
30. Ukrainian Nature Conservation Group The Consequences of the Russian Terrorist Attack on the Kakhovka Hydroelectric Power Plant (HPP) for Wildlife. Available online: https://uncg.org.ua/en/the-consequences-of-the-russian-terrorist-attack-on-the-kakhovka-hydroelectric-power-station-hps-for-wildlife/ (accessed on 11 April 2024).

Disclaimer/Publisher's Note: The statements, opinions and data contained in all publications are solely those of the individual author(s) and contributor(s) and not of MDPI and/or the editor(s). MDPI and/or the editor(s) disclaim responsibility for any injury to people or property resulting from any ideas, methods, instructions or products referred to in the content.